Journal of Medicinal Chemistry

pubs.acs.org/jmc

Article

Enhancing the Pharmacokinetics and Antitumor Activity of an α-Amanitin-Based Small-Molecule Drug Conjugate via Conjugation with an Fc Domain

Francesca Gallo,[§] Barbara Korsak,[§] Christoph Müller, Torsten Hechler, Desislava Yanakieva, Olga Avrutina, Harald Kolmar, and Andreas Pahl*

Cite This: *J. Med. Chem.* 2021, 64, 4117−4129

Read Online

ACCESS | Metrics & More | Article Recommendations | Supporting Information

ABSTRACT: Herein we describe the design and biological evaluation of a novel antitumor therapeutic platform that combines the most favorable properties of small-molecule drug conjugates (SMDCs) and antibody drug conjugates (ADCs). Although the small size of SMDCs, compared to ADCs, is an appealing feature for their application in the treatment of solid tumors, SMDCs usually suffer from poor pharmacokinetics, which severely limits their therapeutic efficacy. To overcome this limitation, in this proof-of-concept study we grafted an α-amanitin-based SMDC that targets prostate cancer cells onto an immunoglobulin Fc domain via a two-step "program and arm" chemoenzymatic strategy. We demonstrated the superior pharmacokinetic properties and therapeutic efficacy of the resulting Fc-SMDC over the SMDC in a prostate cancer xenograft mouse model. This approach may provide a general strategy toward effective antitumor therapeutics combining small size with pharmacokinetic properties close to those of an ADC.

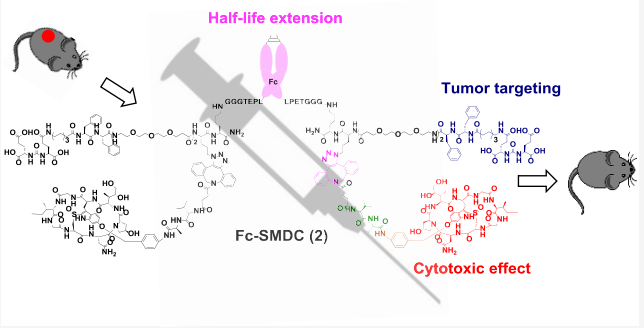

INTRODUCTION

Antibody drug conjugates (ADCs), which use monoclonal antibodies as tumor-homing vehicles for site-specific delivery of cytotoxic drugs to the tumor tissue, represent a breakthrough in cancer treatment.[1] By recognizing tumor-associated antigens with high specificity, ADCs deliver cytotoxic drugs to the tumor site and reduce the systemic toxicities often caused by conventional chemotherapy. Despite the success of trastuzumab-emtansine in breast cancer treatment,[2] the clinical implementation of ADCs for the therapy of solid malignancies is still hampered by the poor penetration of full format antibodies in the solid tumor tissue.[3] Small-molecule drug conjugates (SMDCs) based on small organic ligands as tumor-homing vehicles have been recently gaining growing attention due to their advanced tumor penetration, in contrast to high-molecular-weight ADCs. Promising results have been achieved in the preclinical setting with SMDCs targeting a limited number of receptors, i.e., the folate receptor,[4] the prostate-specific membrane antigen (PSMA),[5,6] the somatostatin receptors,[7] and the carbonic anhydrase IX (CIX).[8]

On the one hand, SMDCs might penetrate solid tumor tissue better due to their small molecular size compared to ADCs. On the other hand, the small size of SMDCs is the main reason for their extremely short half-life in circulation, which in turn limits their gradual tumor uptake and compromises their therapeutic efficacy.[8] Prolongation of the circulatory half-life is required to turn SMDCs into effective anticancer therapeutics. Conjugation to Fc fragments has been successfully applied to limit renal clearance of small molecules by increasing their molecular size and exploiting the Fc receptor (FcRn) recycling process responsible for the long half-life of immunoglobulin G antibodies (IgGs) in circulation.[9,10] Introduction of an Fc portion in the structure of active pharmacological proteins or peptides such as etanercept and romiplostin enabled their therapeutic use by optimization of pharmacokinetic properties, namely, prolongation of circulatory half-life.[11] In this proof-of-concept study, we grafted a SMDC onto an IgG1-Fc scaffold and compared the therapeutic efficacy of this novel small-molecule-Fc-drug conjugate (Fc-SMDC) with that of a PSMA-targeting SMDC lacking the Fc portion. We hypothesized that by grafting the SMDC onto an IgG1-Fc scaffold, the novel product would display a prolonged half-life in circulation compared to the SMDC, allowing for a gradual cytotoxic drug

Received: January 1, 2021
Published: March 23, 2021

https://doi.org/10.1021/acs.jmedchem.1c00003
J. Med. Chem. 2021, 64, 4117−4129

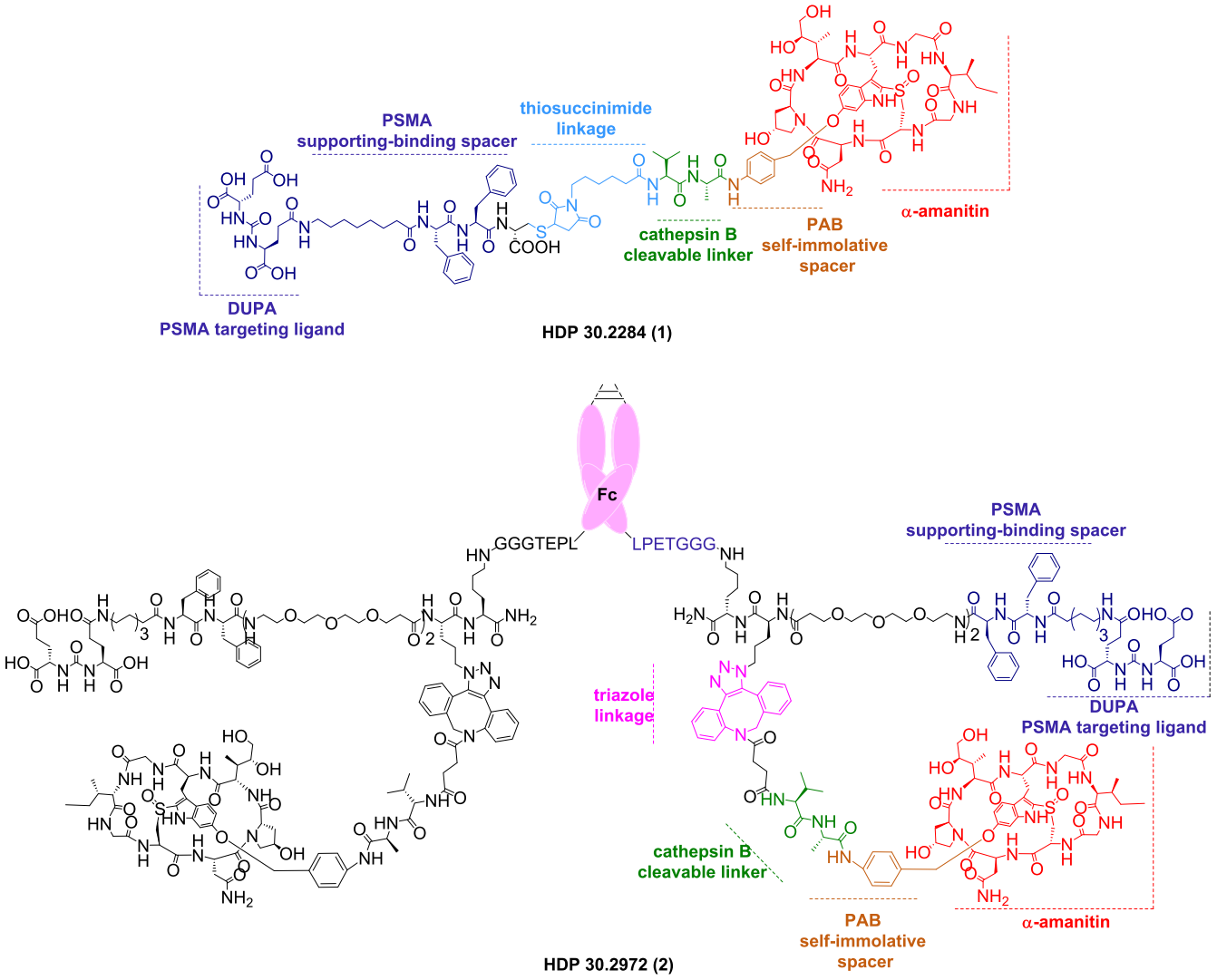

Figure 1. Structures of the SMDC and Fc-SMDC targeting PSMA. Molecules are color-coded as follows: PSMA-targeting ligand, L-Glu-urea-L-Glu (DUPA, blue); PSMA supporting−binding spacer 8-Aoc-Phe-Phe (Pep, blue); thiosuccinimide (HDP 30.2284, cyan) or triazole (HDP 30.2972, magenta) linkage; cathepsin B cleavable linker Val-Ala (green); PAB self-immolative spacer (orange); and α-amanitin (red).

accumulation in the tumor tissue and enhanced antitumor efficacy.

To the best of our knowledge, this is the first report proposing the chemical grafting onto the Fc scaffold of both: a targeting moiety for providing target selectivity and a cytotoxic payload for exerting an antitumor effect. The constructs investigated in the present study have been designed to target prostate cancer (PCa) cells via a glutamate-urea-based targeting motif that binds to the prostate-specific membrane antigen (PSMA) with high affinity. PSMA is a transmembrane glycoprotein overexpressed by virtually all PCas[12] and on the neovasculature of other solid tumors.[13] The same PSMA-targeting motif was explored in clinical trials with a tubulysin B-based SMDC product, EC1169.[14] PSMA-targeted ADCs based on microtubule inhibitors and DNA-cross-linkers were also investigated in the clinical setting of prostate cancer therapy with limited success.[15,16]

The discontinuation of clinical development of some ADCs based on microtubule inhibitors for solid cancer indications[16] prompted us to investigate a toxic payload with an alternative mode of action distinct from currently used toxic payloads[17] and more favorable physicochemical properties, namely, α-amanitin. α-Amanitin is a bicyclic octapeptide isolated from the green death cap mushroom *Amanita phalloides*, which acts as a potent RNA polymerase II inhibitor in eukaryotic cells, significantly slowing down the rate of transcription.[18] In contrast to the majority of applied payloads, α-amanitin kills both dividing and nondividing cells enabling the respective conjugates to eradicate dormant tumor cells and thus preventing tumor recurrence and metastasis. Additionally, its hydrophilic nature excludes cell permeation via passive diffusion and requires receptor-mediated internalization to exert its cytotoxic activity. This makes α-amanitin appealing from the safety perspective.[18] We expected that the combination within a single platform of (1) a small organic ligand with efficient targeting and internalization properties, (2) a hydrophilic payload possessing a unique mode of action, and (3) an Fc portion conferring extended circulatory half-life would lead to an ADC-like therapeutic agent with effective antitumor activity yet much smaller in size.

RESULTS

The design of an SMDC construct targeting PSMA started with the selection of a small molecule capable of binding

https://doi.org/10.1021/acs.jmedchem.1c00003
J. Med. Chem. 2021, 64, 4117−4129

Scheme 1. Synthesis of the PSMA-Targeting Sequence[a]

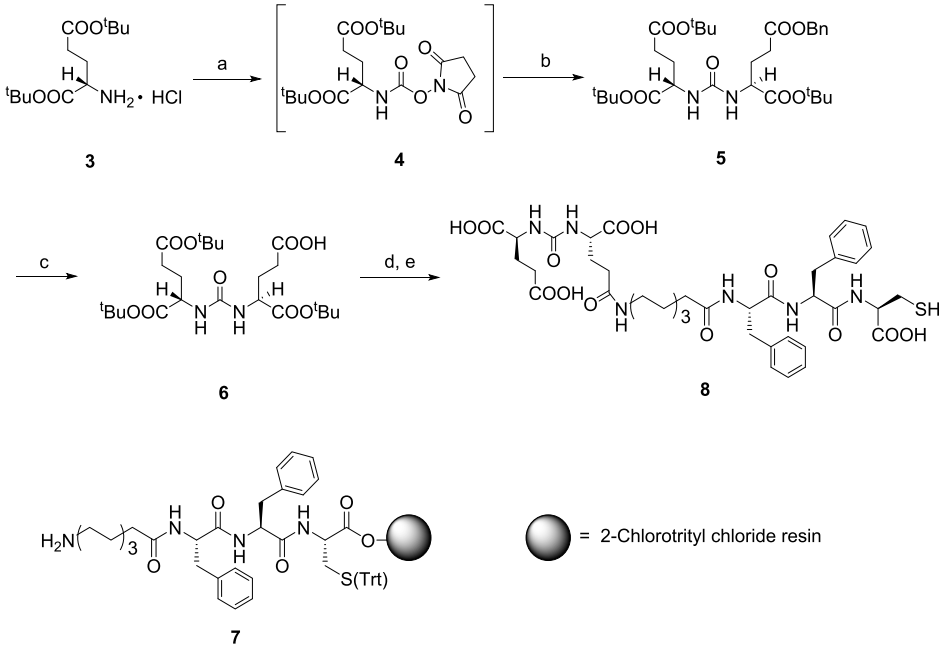

[a]Reagents and conditions: (a) H-Glu(O^{t}Bu)-O^{t}Bu, DSC, TEA, DMF, and 0 °C; (b) H-Glu(OBn)-O^{t}Bu, TEA, DMF, 0 °C to rt, and 77%; (c) H_2, Pd-C, EtOAc, rt, and 96%; (d) **7**, HBTU/HOBt, DIPEA, 40 W, and 60 °C; and (e) TFA/TIPS/H_2O/DTT, rt, and 68%.

Scheme 2. Synthesis of SMDC 1 and the Drug-Linker Payload 12[a]

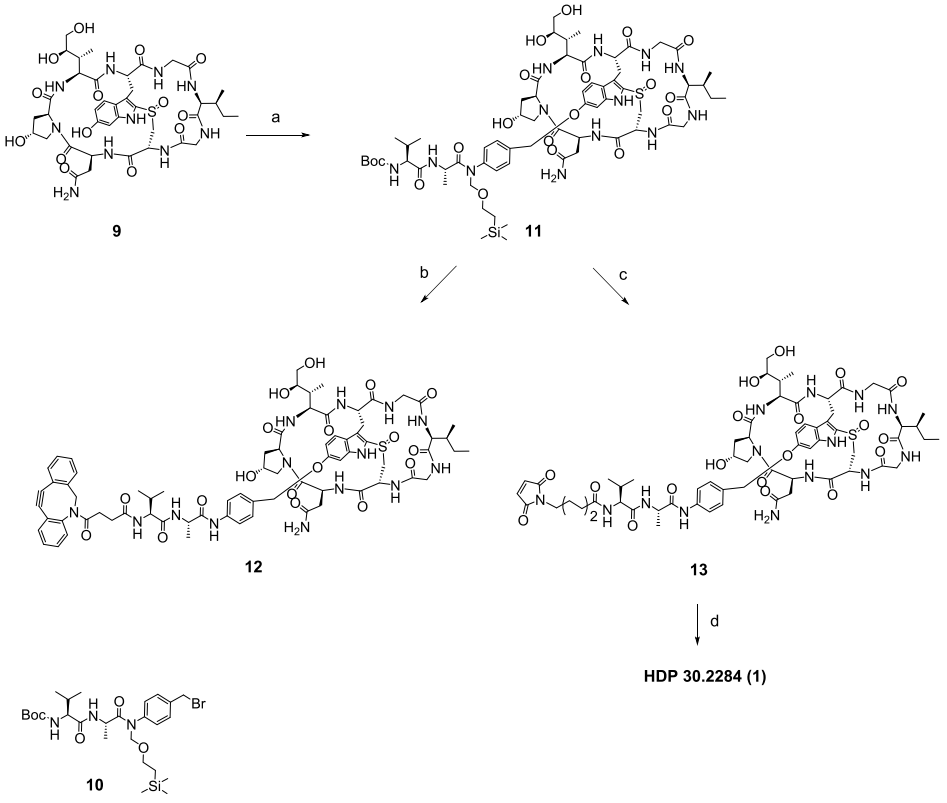

[a]Reagents and conditions: (a) **10**, Cs_2CO_{3aq}, DMA, Ar, rt, and 62%; (b) (1) TFA, 2 min, and rt; (2) NH_{3aq} pH 10, and rt; and (3) DBCO-NHS, DIPEA, DMF, Ar, rt, and 86%; (c) (1) TFA, 2 min, and rt; (2) NH_{3aq} pH 10; and (3) ECMS, DIPEA, DMF, Ar, rt, and 86%; and (d) **8**, DIPEA, DMSO, Ar, rt, and 43%.

PSMA and enhancing its constitutive internalization.[19] The glutamate-urea-based ligand DUPA (2-[3-(1,3-dicarboxyprop-yl)-ureido]pentanedioic acid) was proven to bind to PSMA with high affinity (K_i = 8 nM; IC_{50} = 47 nM) and carry its cargo into PSMA-expressing cells via receptor-mediated endocytosis.[5]

https://doi.org/10.1021/acs.jmedchem.1c00003
J. Med. Chem. 2021, 64, 4117−4129

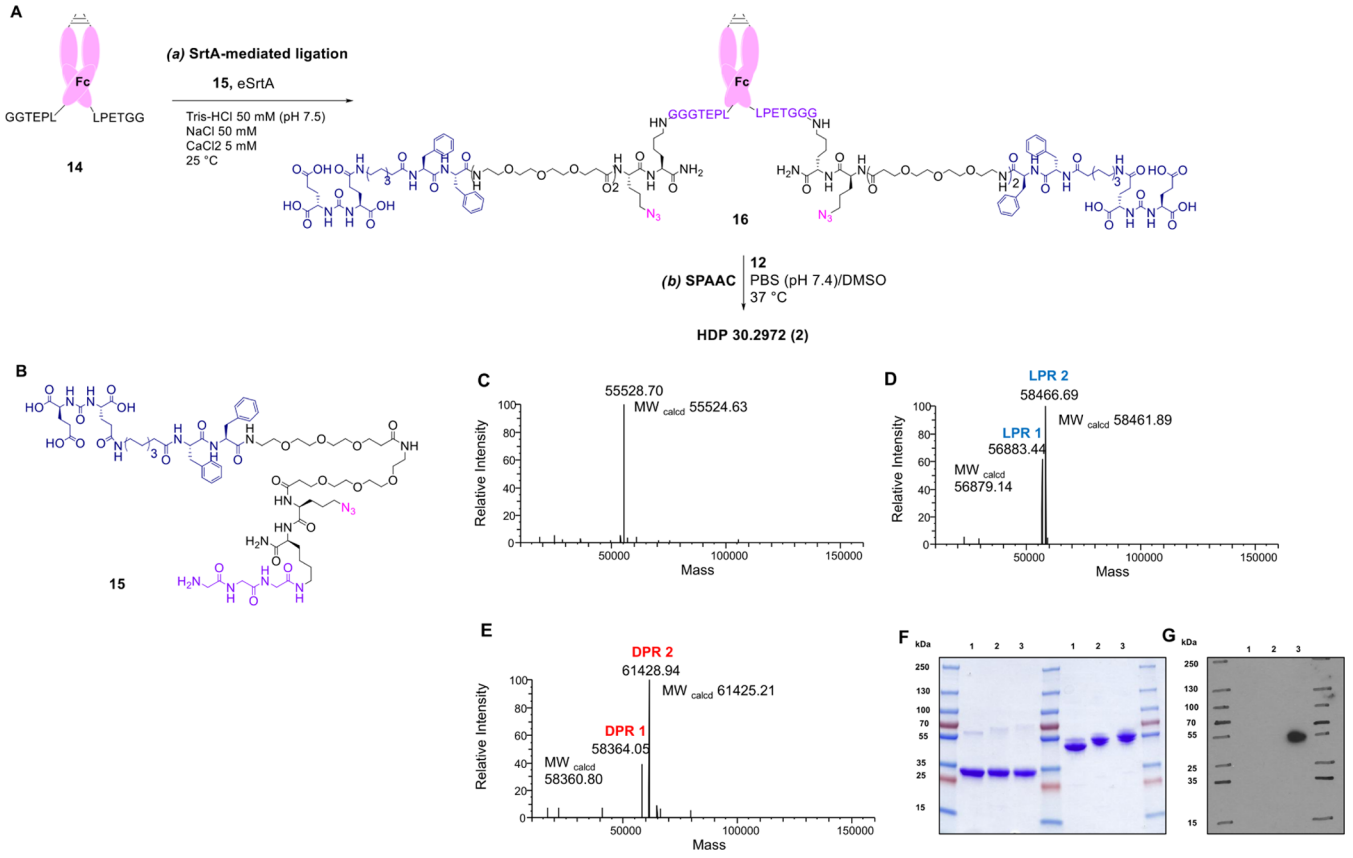

Figure 2. Strategy for programming and arming the Fc scaffold and characterization of Fc-SMDC HDP 30.2972. (A) Step a: the IgG1-Fc-LPETGG scaffold (14) is programmed by attaching at the C-terminus the trifunctional linker 15 (B) containing the DUPA-Pep PSMA binding sequence (blue) and an azide as "clickable" handle (magenta) through sortase A (eSrtA)-mediated ligation; step b: the programmed DUPA-Pep-Fc 16 is armed with the dibenzocyclooctine (DBCO)-Val-Ala-PAB-α-amanitin payload (12) via strain-promoted azide-alkyne cycloaddition (SPAAC). HRESI-MS analysis after deconvolution of (C) IgG1-Fc-LPETGG (14), (D) DUPA-Pep-Fc 16, and (E) DUPA-Pep-Fc-α-amanitin Fc-SMDC (2, HDP 30.2972). (F) SDS-PAGE analysis under reducing and nonreducing conditions and (G) anti-α-amanitin Western blot under nonreducing conditions. SDS-PAGE was performed on Fc-LPETGG (14; lane 1), DUPA-Pep-Fc (16; lane 2), and DUPA-Pep-Fc-α-amanitin Fc-SMDC (2, HDP 30.2972, lane 3), followed by staining with Coomassie blue or Western blot analysis with immunodetection of α-amanitin. Pep = 8-Aoc-Phe-Phe, LPR = linker-to-protein ratio, and DPR = drug-to-protein ratio.

A growing body of evidence shows that the overall binding to PSMA can be enhanced by introducing a supporting−binding spacer that fits the structural contour and chemical environment of the gradually narrowing 20 Å tunnel, which accesses the PSMA binding site. The supporting−binding spacer 8-Aoc-Phe-Phe, henceforth referred to as Pep, as shown by Kularatne et al., enhances the binding affinity of a DUPA analogue by a factor of 6 and therefore was used in combination with DUPA (DUPA-Pep) for targeting PSMA.[19] As shown in Figure 1, the SMDC **HDP 30.2284 (1)** comprises the binding sequence DUPA-Pep (shown in blue) conjugated to the cytotoxic drug payload (shown in red) via a thiosuccinimide linkage (shown in cyan) through a dipeptide Val-Ala linker (shown in green). The dipeptide Val-Ala is a substrate for the lysosomal cathepsin B, a proteolytic enzyme overexpressed in tumor cells.[20,21] To ensure cleavage of the Val-Ala motif for release of the free toxin, a self-immolative *p*-aminobenzyloxy spacer (PAB; Figure 1, shown in orange) was introduced between the toxin and the dipeptide linker. The SMDC grafted onto the IgG1-Fc scaffold was designed as an **HDP 30.2284** analogue. However, thiosuccinimide-linked conjugates might be susceptible to drug loss over time through a retro-Michael addition or thiol exchange reactions in thiol-containing environments.[22] Thus, in **HDP 30.2972 (2)**, we used the more stable triazole linkage instead of the thiosuccinimide (Figure 1, shown in magenta) to anchor the α-amanitin payload with the Fc framework. Furthermore, to avoid steric interference with the large Fc protein, a flexible EG_3 (ethylene glycol) dimer was introduced as spacer between the targeting motif and the drug-linker payload. The hydrophilicity of the $(EG_3)_2$ spacer provided an additional advantage by increasing the water solubility of the synthetic component enabling conjugation in aqueous media. As outlined in Scheme 1, the DUPA precursor (**6**) was synthesized according to the procedure reported by Kularatne et al.[19] with minor modifications toward easier handling conditions. The commercially available *tert*-butyl glutamic acid **3** was first activated as succidimidyl ester **4**. Following the addition of γ-benzylated glutamic acid, the fully protected DUPA intermediate **5** was hydrogenated yielding the DUPA precursor **6**. Acylation of the resin-bound peptide **7** (synthesized using Fmoc-based solid-phase peptide chemistry) with precursor **6** was followed by resin cleavage and global deprotection yielding the DUPA-Pep binding sequence **8**. The binding sequence **8** bears a C-terminal cysteine to address the maleimide-containing drug-linker payload. The approach to access SMDC **1** is outlined in Scheme 2. The key step is the formation of an ether bond through alkylation of the phenolic

https://doi.org/10.1021/acs.jmedchem.1c00003
J. Med. Chem. 2021, 64, 4117−4129

6′-hydroxy group in the tryptophan residue of natural α-amanitin with bromide **10**. Following alkylation, the α-amanitin derivative **11** was subjected to a two-step protocol involving global deprotection and functionalization with *N*-maleimidocaproyl-oxysuccinimide ester (ECMS). The resulting α-amanitin derivative **13** was then coupled with the DUPA-Pep sequence **8** affording SMDC **HDP 30.2284 (1)** in 43% yield. For grafting the SMDC product onto a human IgG1-Fc scaffold, a two-step "program and arm" strategy (Figure 2) was developed.[23]

The IgG1-Fc scaffold was first programmed by attaching the trifunctional linker **15** simultaneously bearing the cell-specific targeting motif DUPA-Pep (shown in blue), an N-terminal oligoglycine substrate for the regiospecific labeling of the Fc scaffold (purple), and a clickable handle (magenta, Figure 2B) for subsequent arming with the toxin payload **12**. To generate a product with a defined drug-to-protein ratio (DPR) of 2, the human IgG1-Fc scaffold was equipped at the C-termini with the peptide tag LPETGG allowing for Fc programming via sortase A (SrtA)-mediated ligation. SrtA is a transpeptidase from *Staphylococcus aureus* widely used for site-specific modifications of antibodies and antibody fragments[24−27] that catalyzes the formation of a new amide bond between the C-terminal sorting motif LPXTG (where X is equal to any amino acid) and an N-terminal oligoglycine (G)*n* (*n* = 3−5) nucleophile. The programmed DUPA-Pep-Fc conjugate (**16**, Figure 2A) was confirmed to be a disulfide-linked Fc dimer by SDS-PAGE under reducing and nonreducing conditions (Figure 2F). HRESI-MS analysis under nonreducing conditions (Figure 2D) further confirmed the expected molecular weight for an Fc dimer. Deconvolution results revealed two different peaks, which were assigned to versions of the Fc dimer modified with one to two molecules of the trifunctional linker **15**, resulting in an average linker-to-protein ratio (LPR) of 1.62 (Figure 2D). Following the SrtA-mediated ligation, the strain-promoted azide-alkyne cycloaddition (SPAAC; Figure 2A, step b) was explored to conjugate the drug-linker component **12** (Scheme 2). The chemoselective copper-free click chemistry was chosen to minimize protein oxidation by reactive oxygen species and to avoid residual copper in the final product, therefore preventing potential copper-related cytotoxicity. As shown in Scheme 2, the drug-linker component **12** was obtained in 86% yield from the intermediate **11** upon global deprotection and coupling to DBCO-NHS ester. Incorporation of α-amanitin in the final product **2** (**HDP 30.2972**) was confirmed by SDS-PAGE under nonreducing conditions (Figure 2F), showing signal migration to higher molecular weight (lane 3) in comparison to DUPA-Pep-Fc (**16**; lane 2) and by Western blot analysis with immunodetection of α-amanitin (Figure 2G). Heterogeneity of the DUPA-Pep-Fc precursor **16** with respect to the number of attached linker molecules led to the formation of heterogeneous species with a drug-to-protein ratio (DPR) ranging from 1 to 2, as confirmed by the deconvoluted mass spectrum (Figure 2E). The average DPR was calculated to be 1.72, consistent with the LPR value reported for precursor **16** (Figure 2D). Importantly, no species loaded with the linker but not conjugated to the toxin, which could compete with **HDP 30.2972** for binding to either FcRn or PSMA, were detected. Initial *in vitro* characterization of SMDC **HDP 30.2284 (1)** and the chemically programmed and armed Fc-SMDC **HDP 30.2792 (2)** was carried out in the LNCaP cell line overexpressing the targeted receptor. Both conjugates demonstrated high *in vitro* activity in PSMA-positive cells. **HDP 30.2284 (1)** displayed 555-fold higher activity than the unconjugated α-amanitin (IC_{50} 0.863 vs 479 nM) (Figure 3A,C). Compared to **HDP 30.2284 (1)**, Fc-SMDC **HDP 30.2972 (2)** was approximately 17-fold less active, showing an IC_{50} of 15.2 nM (Figure 3). To further confirm that activity of both PSMA-targeted conjugates (**1** and **2**) was receptor-mediated, the cytotoxic potential of the conjugates was determined in the presence of a 100-fold (**HDP 30.2284**, **1**) or a 200-fold (**HDP 30.2972**, **2**) molar excess of 2-PMPA, a well-known inhibitor of PSMA enzymatic activity and a competitive inhibitor of DUPA.[5] Under these conditions, the cytotoxic activity of both conjugates in LNCaP cells was completely inhibited. Further biological characterization of conjugates **HDP 30.2284 (1)** and **HDP 30.2972 (2)** was focused on *in vivo* studies: determination of the maximum tolerated dose, pharmacokinetics and biodistribution, and antitumor efficacy. In mice, the maximum tolerated dose (MTD) was found to be 0.046 mg/kg (18.74 μg/kg of α-amanitin) for **HDP 30.2284 (1)** and 1.0 mg/kg (25.7 μg/kg of α amanitin) for **HDP 30.2972 (2)**. Biodistribution of both conjugates was monitored to follow blood pharmacokinetics and accumulation in tumor, liver, and kidneys. For pharmacokinetic analyses, animals were injected with a dose corresponding to 4× MTD (0.184 mg/kg) of **HDP 30.2284 (1)** to secure detectable concentrations of the conjugate in the serum and the organ extracts. For the quantitation of the

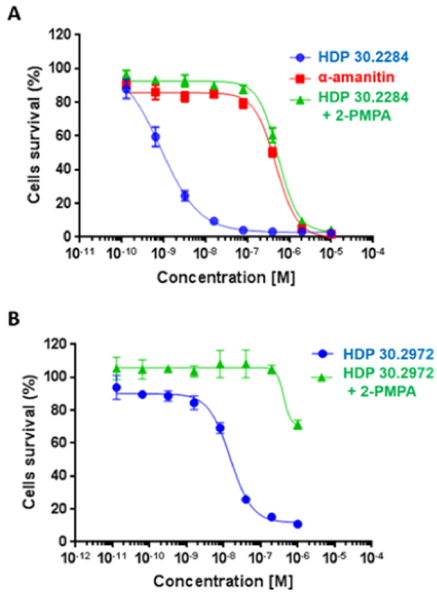

Tested compound	IC_{50} (nM)
HDP 30.2284	0.863
HDP 30.2284 + 2-PMPA	540
HDP 30.2972	15.2
HDP 30.2972 + 2-PMPA	n.d.
α-amanitin	479

Figure 3. Cytotoxicity of SMDC HDP 30.2284, Fc-SMDC HDP 30.2972, and unconjugated α-amanitin in the PSMA-positive LNCaP (PSMA +++) cell line. Both conjugates were tested in the presence or the absence of 2-PMPA excess, a competitive inhibitor of PSMA. (A) Dose-response cytotoxic potential of HDP 30.2284. (B) Dose-response cytotoxic potential of HDP 30.2972. (C) Tabular summary of the IC_{50} values (data shown are mean ± SEM; *n* = 3).

https://doi.org/10.1021/acs.jmedchem.1c00003
J. Med. Chem. 2021, 64, 4117−4129

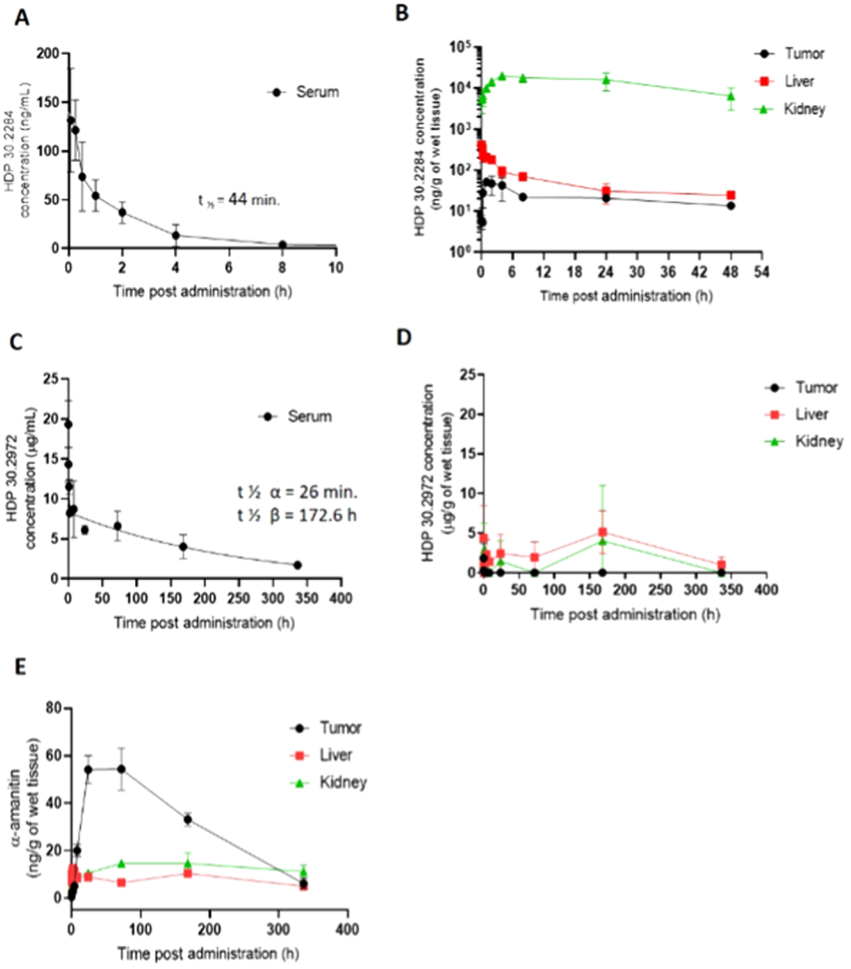

Figure 4. Pharmacokinetic profile and biodistribution of SMDC HDP 30.2284 and Fc-SMDC HDP 30.2972. (A) Blood pharmacokinetics of HDP 30.2284 with the indicated $t_{1/2}$ after single-dose administration of 0.184 mg/kg (CB17-Scid mice, mean concentration ± SEM, n = 3). (B) Biodistribution of HDP 30.2284 in the tumor, liver, and kidney after single-dose administration of 0.184 mg/kg (CB17-Scid xenografted with LNCaP tumors, mean concentration ± SEM, n = 3). (C) Blood pharmacokinetics of HDP 30.2972 after single-dose administration of 1 mg/kg, (CB17-Scid xenografted with LNCaP tumors, mean concentration ± SEM, n = 3). (D) Biodistribution of HDP 30.2972 after single-dose administration of 1 mg/kg (CB17-Scid xenografted with LNCaP tumors, mean concentration ± SEM, n = 3). (E) Concentration of free α-amanitin released from HDP 30.2972 after a single i.v. dose of 1 mg/kg in the tumor, liver, and kidney (CB17-Scid xenografted with LNCaP tumors, mean concentration ± SEM, n = 3). No free α-amanitin was detected in the serum after administration of HDP 30.2972 (data not shown).

conjugate, we used an anti-α-amanitin ELISA, which detects the parent compound **HDP 30.2284**, as well as all possible metabolites presenting α-amanitin in the structure. Serum levels of **HDP 30.2284 (1)** rapidly declined and were below the lower limit of quantification 24 h and 48 h after administration (Figure 4A,B). The concentration of **HDP 30.2284 (1)** in the tumor reached its maximum (approx. 50 ng/g) 1 h after administration, and a much lower concentration of only approx. 2 ng/g 48 h after administration (Figure 4B). These results suggested that in a subsequent *in vivo* antitumor efficacy study, a high administration frequency should be applied to increase the exposure and provide higher levels of tumor accumulation. Overall, a high conjugate concentration was found in the liver reflecting the blood concentration due to the high congestion of this organ. Despite complete elimination from circulation, a concentration of approx. 20 ng/g was detected in the liver 48 h after administration. In contrast to the low concentrations of the toxin detected in the tumor and the liver, very high concentrations were observed in the kidney throughout duration of the study. A peak concentration of approx. 2.0 μg/g was observed 4 h after single-dose administration and was followed by a slight drop to approx. 1.0 μg/g, detectable 48 h after administration. These results suggested a high accumulation of the conjugate in the kidney. The *in vivo* pharmacokinetics of Fc-SMDC **HDP 30.2972 (2)** was determined at a dose corresponding to the MTD (1 mg/kg). The pharmacokinetic analysis revealed that with a size lower than that of a conventional ADC (approx. 61 vs 150 kDa, respectively), Fc-SMDC **HDP 30.2972 (2)** showed ADC-like pharmacokinetic properties and a much longer circulatory half-life compared to SMDC **HDP 30.2284 (1)**. Fc-SMDC **HDP 30.2972 (2)** displayed a biphasic elimination profile typical for molecules harboring an Fc motif (Figure 4C). Fast (α-phase) and slow (β-phase) elimination half-lives were determined to be 26 min and 172.6 h (approx. 7.2 days), respectively (Figure 4C).

In the liver and the kidney, a low concentration throughout duration of the study was detected with a transient increase observed at day 7 (Figure 4D). Detectable levels of intact **HDP 30.2972 (2)** were present in the tumor only 5 and 15 min after administration. For the remaining time-points, the concen-

https://doi.org/10.1021/acs.jmedchem.1c00003
J. Med. Chem. 2021, 64, 4117−4129

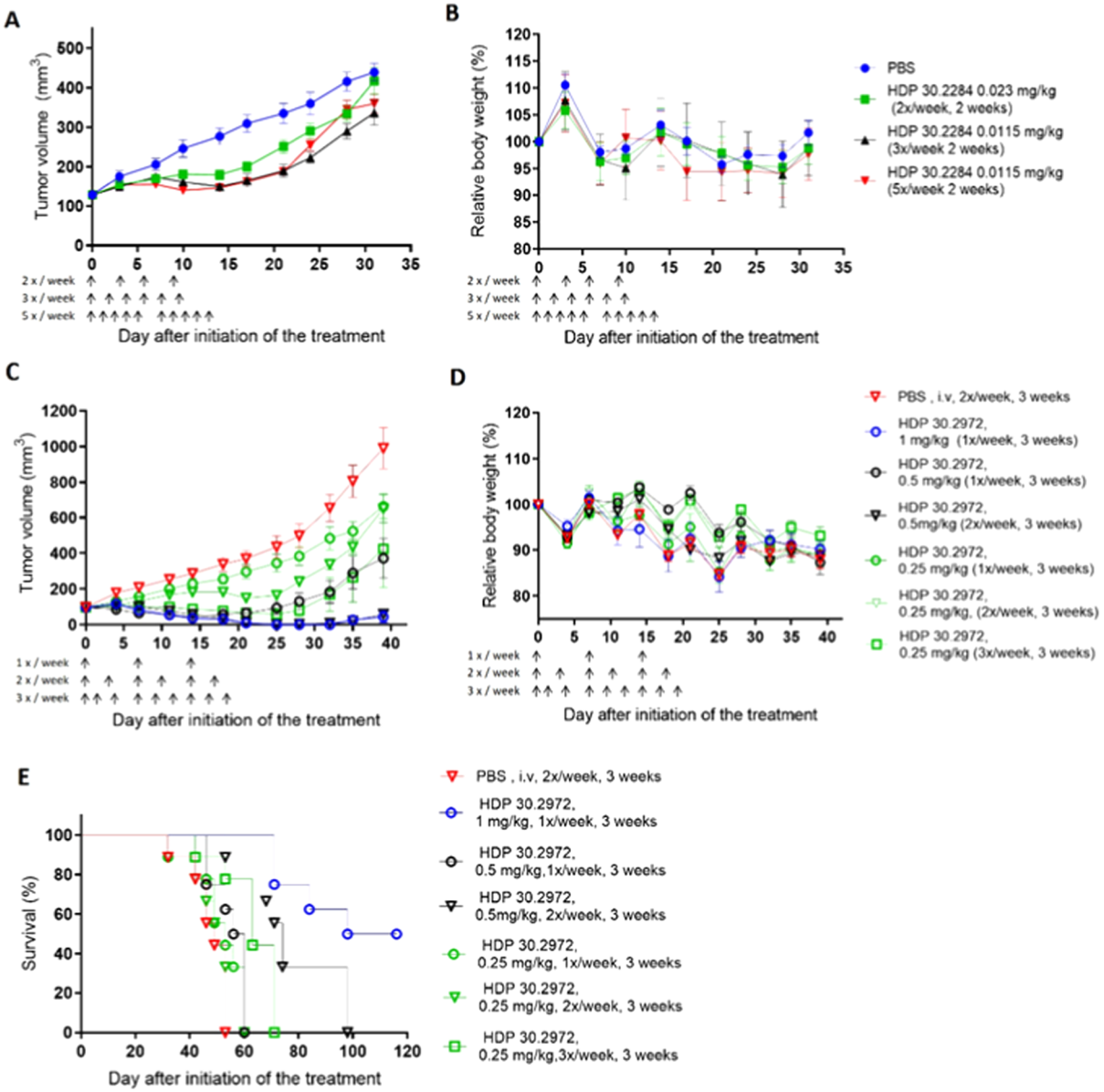

Figure 5. *In vivo* antitumor activity and tolerability of SMDC HDP 30.2884 and Fc-SMDC HDP 30.2972. (A) Efficacy of the therapy with HDP 30.2284. (B) Tolerability of HDP 30.2284. (C) Efficacy of the therapy with HDP 30.2972. (D) Tolerability of HDP 30.2972. (E) Long-term survival follow-up of the animals treated with HDP 30.2972. The mean tumor volume ± SEM is shown for the efficacy experiment and the median body weight ± SEM for tolerability graphs (n = 8−9).

tration of intact conjugate in the tumor was below lower limit of quantification. The Val-Ala-PAB linker was designed to be cleaved inside of the cells via intracellular cathepsin B. To determine the concentration of the released payload, the concentration of free α-amanitin in the same tissue samples was measured using an anti-α-amanitin ELISA. The serum concentration of the released toxin was below lower limit of quantification throughout the study duration, which is evidence of high conjugate stability in the circulation (data not shown). Only minimal variation in α-amanitin levels over time was observed in the liver and the kidney (Figure 4E). The maximum concentration of 14 ng/g was measured in the kidney 72 h after **HDP 30.2972 (2)** administration and remained at a similar level up to 14 days following administration. The concentration of the unconjugated toxin detected in the kidney was slightly higher than that in the liver (Figure 4E). Most importantly, the highest concentration of the released toxin was found in the tumor with the peak concentration of approx. 54 ng/g measured at days 1 and 3 after administration. At day 7, the tumor toxin concentration dropped slightly to 33 ng/g but was still detectable in the tumor tissue even 14 days after single-dose administration (Figure 4E). Next, the therapeutic activities of both SMDC (**1**) and Fc-SMDC (**2**) were tested in CB17-Scid male mice implanted with PSMA-positive LNCaP tumors. Frequent dosing of **HDP 30.2284 (1)** was applied to provide high exposure and compensate for the short half-life of this compound (Figure 5A). Treatment with **HDP 30.2284 (1)** led to limited tumor regression at all doses, with the lowest efficacy observed at 0.023 mg/kg (1/2 MTD) 2×/week, while the intermediate efficacy and the highest antitumor activity were observed at 0.0115 mg/kg (1/4 MTD) 5×/week and 0.0115 mg/kg (1/4 MTD) 3×/week, respectively (Figure 5A).

https://doi.org/10.1021/acs.jmedchem.1c00003
J. Med. Chem. 2021, 64, 4117−4129

All dosing regimens were well tolerated as indicated by only minor losses in the relative body weight (Figure 5B). Despite transient tumor-growth inhibition, after cessation of the therapy, tumors in all groups treated with **HDP 30.2284 (1)** started to regrow with kinetics similar to that of the vehicle-injected group. Doses and the frequency of **HDP 30.2972 (2)** administration were based on the pharmacokinetic profile and MTD studies of this compound (Figure 5C,5D). The antitumor effect of **HDP 30.2972 (2)** was dose-dependent (Figure 5C).

While a dose of 1 mg/kg led to complete remission, the 0.25 mg/kg dose was hardly effective, and the 0.5 mg/kg dose showed intermediate efficacy (Figure 5C). Furthermore, a dosing frequency-dependent effect was observed in the groups dosed with 0.25 mg/kg, whereas the three-times-per-week regimen led to the highest tumor response. The tumor volume of the group administered with 0.5 mg/kg once per week converges with the tumor volume of the group administered with 0.25 mg/kg three times per week, but 0.25 mg/kg twice per week was less efficacious than 0.5 mg/kg once a week (Figure 5C). Although a very similar tumor response was observed for 1 mg/kg administered once per week and 0.5 mg/kg administered twice per week, a higher number of durable complete responses was observed for the animals dosed with 1 mg/kg. In the long-term follow-up, all animals dosed with 0.5 mg/kg twice per week experienced tumor relapse and had to be sacrificed due to unacceptably high tumor volume (Figure 5E). In contrast, at day 116 following initiation of the therapy, 4 out of 8 animals from the group treated once per week with 1 mg/kg were still alive, demonstrating complete response and significantly longer median survival (Figure 5E).

DISCUSSION

Despite representing a breakthrough in cancer treatment, challenges still remain for application of ADCs to difficult-to-treat solid tumors, due to the specific tumor physiology and poor ADC penetration in the tumor mass. From this perspective, SMDCs may potentially achieve better penetration in the tumor tissue. Additionally, the design of a conjugate that is able to eradicate the tumor and overcome tumor-resistance and off-target toxicity issues may benefit from the application of payloads with alternative modes of action and more favorable physicochemical properties.

In the present study, we combined the tumor-homing properties of the small-molecule DUPA targeting PSMA with the novel mode of action of α-amanitin, a potent RNA polymerase II inhibitor, for the treatment of PCa. However, SMDCs suffer from a short circulation half-life because of their small size, limiting the conjugate tumor uptake and efficacy.[28] Hence, an attempt was made to design a small format conjugate with improved pharmacokinetic properties and therapeutic activity by grafting the SMDC onto an IgG1-Fc fragment, leading to the novel Fc-SMDC format. The SMDC and Fc-SMDC products were then compared in the *in vitro* and *in vivo* settings.

In terms of the *in vitro* cytotoxic activity, both SMDC **1** (IC_{50} 0.863 nM) and Fc-SMDC **2** (IC_{50} 15.2 nM) outperformed unconjugated α-amanitin (IC_{50} 476 nM) and stood out as having selective activity in a low nanomolar range of concentration (Figure 3). The low *in vitro* activity displayed by unconjugated α-amanitin is related to its hydrophilic properties and the inability to passively penetrate the cell membrane in the absence of a homing vehicle that shuttles it into cells.[18] This is in contrast to the majority of currently used in the development of ADCs and SMDCs payloads, which are highly hydrophobic and able to induce cytotoxicity and antitumor activity even in the absence of receptor-mediated internalization as a consequence of possible premature linker cleavage and passive uptake.[29,30] Premature linker cleavage and release of the hydrophobic cytotoxic payload is the main reason for off-target toxicities. In the case of ADCs, the conjugation of such payloads to large hydrophilic antibodies via stable linkers can mitigate unspecific uptake and reduce the risk of systemic toxicity. On the contrary, the conjugation to low-molecular-weight ligands is not expected to have an influence on the payload physicochemical properties sufficient to avoid an unspecific uptake. In several studies, it was demonstrated that SMDCs featuring hydrophobic toxins such as tubulysin B, MMAE, or paclitaxel show cytotoxic potentials in a concentration range similar to those observed for the unconjugated toxins,[5,31,32] supporting the hypothesis of passive toxin cellular uptake despite conjugation to a small targeting molecule. However, in our experiments, a remarkably lower potential was observed in PSMA-negative PC3 cells for both tested compounds, further confirming a PSMA-mediated uptake (Supporting Information Figure S4). Cytotoxicity experiments performed in the presence of the competitive inhibitor 2-PMPA ultimately confirmed that receptor-mediated internalization is essential to unfold the cytotoxic potential of α-amanitin. To the best of our knowledge, α-amanitin-based SMDCs described in the literature so far demonstrated only 4−5-fold better targeting properties compared to the unconjugated toxin.[33,34] Here, we report for the first time a tremendous increase in the activity of α-amanitin upon conjugation to a small-molecule tumor-targeting ligand. A comparative pharmacokinetic and biodistribution study revealed significant differences in the half-life, tumor, and organ accumulation of SMDC **(1)** and Fc-SMDC **(2)** products. The small size of **HDP 30.2284 (1)** and the consequent rapid glomerular filtration accounts for its short *in vivo* half-life of only approx. 44 min (Figure 4A). For Fc-SMDC **(2)**, a blood pharmacokinetic profile typical for molecules presenting an Fc motif in the structure was observed ($t_{1/2}$ α-phase = 26 min and $t_{1/2}$ β-phase = 7.2 days). As the molecular weight of **HDP 30.2972 (2)** slightly exceeds the renal cutoff of 60 kDa, the contribution of renal filtration to its clearance is supposed to be lower than for **HDP 30.2284**. However, engagement of Fc-SMDC **(2)** with the FcRn recycling process, which protects the molecule from proteolytic degradation, retains it in the intracellular compartment and concomitantly protects it from rapid renal clearance and is thus supposed to be most likely the main contribution to the prolongation of half-life.[9] Our strategy resembles available preclinical studies that have demonstrated that clearance of therapeutic peptides fused to an IgG-Fc domain is increased 14- to 24-fold in FcRn-knockout mice compared to wild-type animals.[35,36]

A well-known organ of target toxicity for α-amanitin is the liver. We reasoned that the slight liver uptake of conjugates observed in *in vivo* studies (Figure 4) might be related to the OATP1B3 receptor expressed in liver sinusoids known to be responsible for the α-amanitin transport into the hepatocytes.[37] Heavy accumulation of **HDP 30.2284 (1)** but not **HDP 30.2972 (2)** was observed in the kidneys. Accumulation of DUPA-based molecules in this organ has been reported and is mainly related to the reabsorption via PSMA receptors

https://doi.org/10.1021/acs.jmedchem.1c00003
J. Med. Chem. 2021, 64, 4117−4129

expressed in the proximal tubules of the kidney.[38] Based on literature reports and biodistribution data of **HDP 30.2284 (1)**, the kidneys were identified as the organ of primary toxicity for this molecule. Grafting the DUPA-based SMDC onto the Fc scaffold allowed for not only prolonging the half-life of the conjugate but also significantly limiting the kidney uptake and avoiding accumulation of the toxin in this organ. Different profiles of toxin distribution were observed for the two conjugates investigated in this study. Accumulation of α-amanitin in the tumor over time was observed only after administration of **HDP 30.2972 (2)** but not following administration of **HDP 30.2284 (1)**. These results indicate that only the Fc-SMDC targets the toxin mainly to the tumor where the conjugate is internalized, and the payload is released, leading to a long-lasting antitumor effect.

Compared to SMDC (**1**), the chemically programmed and armed Fc-SMDC (**2**) improved the therapeutic precision and allowed for efficient toxin delivery *in vivo* selectively to cells expressing the targeted PSMA receptor, as confirmed in the *in vivo* efficacy study (Figure 5). Only Fc-SMDC (**2**) allowed for obtaining dose-dependent and long-term *in vivo* antitumor activity. Our results resemble the finding in the field of ADCs, showing that for the cytotoxic payload, a certain intratumoral threshold concentration has to be reached to support sustained efficacy.[39] Additionally, the proof-of-concept study presented herein demonstrates that for conjugates based on hydrophilic payloads like α-amanitin, a prolonged half-life is needed to allow for gradual toxin accumulation in the tumor and achieve a long-lasting antitumor response.

CONCLUSIONS

In the present study, we reported for the first time the conjugation of a SMDC onto a human IgG1-Fc fragment. With a size approximately equal to 40% of conventional ADCs, the novel platform merges the favorable properties of small-sized therapeutics with the PK properties of an ADC.

We demonstrated that, in contrast to the majority of SMDCs that utilize more hydrophobic payloads that are able to passively penetrate tumor cells, SMDCs featuring a hydrophilic payload like α-amanitin are not a suitable format for development of therapeutics for solid-tumor therapy. Prolongation of α-amanitin based SMDSs half-life is necessary to ensure exposure of the target tissue to the hydrophilic drug in the conjugated form, allowing for its gradual uptake and accumulation in the tissue.

The two-step strategy applied here to assemble the Fc-SMDC might become a general approach for the chemical programming and arming of an Fc scaffold. The single generic Fc-LPETGG fragment might be indeed programmed against a variety of targets and be accessible even to chemically synthesized ligands not generally amenable to genetic fusion. Also, such a strategy offers the opportunity to combine different targeting ligands with a variety of linkers, toxic warheads, and conjugation chemistries, thereby expanding the landscape of tumor-targeted technologies.

EXPERIMENTAL SECTION

General Information. Solvents and reagents were purchased from commercial vendors and used without further purification. ESI-MS studies were performed using a Thermo Orbitrap LTQ XL mass spectrometer (Thermo Scientific) connected to an Agilent 1200 series high-performance liquid chromatography (HPLC) system (isocratic mode; mobile phase composition: methanol/acetonitrile/water, 40:40:20; flow rate: 0.25 mL/min). HRESI-MS studies were performed at Immundiagnostik AG (Bensheim, Germany) using an Orbitrap Elite mass spectrometer interfaced with an Ion Max Source (HESI-II probe) (Thermo Scientific) via reverse-phase liquid chromatography (RP-LC) gradient separation. Deconvolution of isotopically unresolved spectra was performed with the ReSpect algorithm using Biopharma Finder 3.0 software (Thermo Scientific). Analytical thin-layer chromatography (TLC) was performed on POLYGRAMSIL G/UV polyester precoated plates (40 × 80 mm^2, 0.20 mm silica gel 60), and compound visualization was accomplished with UV light and ninhydrin or Vaughn's staining reagents. Flash chromatography was carried out using a Teledyne ISCO CombiFlash RF system on Silica RediSep Rf disposable columns. Solid-phase peptide synthesis (SPPS) was performed using the automated microwave peptide synthesizer CEM Liberty Blue or the manual microwave peptide synthesizer CEM Discover System. All peptides and conjugates were purified by preparative RP-HPLC (VWR LaPrep Sigma LP1200 pumps, VWR LaPrep Sigma 3101 UV detector; column: Phenomenex Luna 10 μm C18(2) 100 Å, 250 × 21.2 mm^2) and analyzed by analytical RP-HPLC (VWR Hitachi Chromaster 5110 binary HPLC pump, VWR Hitachi Chromaster 5430 diode array detector (DAD); column: Phenomenex Luna 10 μm C18(2) 100 Å, 250 × 4.6 mm^2). Fc protein was purified by Protein A-based affinity chromatography (Bio-rad NGC 100 Medium-Pressure Chromatography system; column: Tosoh Bioscience ToyoScreen AF-rProtein A HC-650F 5 mL) and dialyzed in Thermo Fisher Scientific Slide-A-Lyzer cassettes (MWCO 20 000, 12−30 mL). Fc-conjugates were purified by preparative size-exclusion fast-protein liquid chromatography (SEC-FPLC, ÄKTA Start system, HiLoad 26/600 Superdex 200 pg column or HiLoad 16/600 Superdex 200 pg column) and analyzed by analytical SEC (Knauer PLATINblue HPLC with DAD, column: Tosoh Bioscience TSKgel UP-SW3000, 2 μm, 4.6 mm ID × 30 cm). Protein and protein-conjugates were concentrated using Amicon Ultra-15 Centrifugal Filters MWCO 50 000 (Millipore) and filtered through disposable 0.22 μm sterile Millex-GV syringe filters (Millipore). Concentration measurements were carried out using a Thermo Fisher Scientific NanoDrop 2000c spectrophotometer (λ = 280, 310 nm, sample size 3 μL). SDS-PAGE analysis was performed on 4−20% precast polyacrylamide gels (Mini-PROTEAN TGX precast protein gel, Bio-rad) in Mini-PROTEAN electrophoresis cells (Bio-rad). Marker PageRuler Plus Prestained Protein Ladder was purchased from Thermo Scientific. Western blot analyses were performed using a primary rabbit α-amanitin polyclonal antiserum (produced at Heidelberg Pharma Research GmbH) probed with an antirabbit IgG-HRP-linked antibody (Cell Signaling Technology). For chemoluminescence detection, Clarity Western ECL substrates (Bio-rad) were used.

General Syntheses. The synthesis route for α-amanitin derivatives **12** and **13** is fully shown in Scheme S1. Starting from natural α-amanitin (**9**), reaction with bromide (**10**) followed by deprotection gave the intermediate **S-1**. The title derivatives were prepared by condensation of the intermediate **S-17** with the appropriate NHS ester-activated cross-linker.

SMDC (1). Compound **8** (12.97 mg, 0.015 mmol) was dissolved in DMSO (1 mL). A solution of **13** (21.03 mg, 0.015 mmol) in DMSO (2 mL) was added at room temperature under argon. DIPEA (5.15 μL, 0.03 mmol) was added undiluted. The reaction mixture was stirred at room temperature for 20 h and then purified by preparative RP-HPLC [λ = 305 nm; gradient: 0−5 min 5% B; 20−25 min 100% B; 27−35 min 5% B; A = water with 0.05% TFA; B = MeOH with 0.05% TFA]. Solvents were evaporated and SMDC **1** was freeze-dried overnight from ^{t}BuOH:H_2O (4:1, v−v; 4 mL) and isolated as a colorless powder (14.53 mg, 43%). MS (ESI): *m/z* calcd for $C_{96}H_{124}N_{20}O_{32}S_2$ + $2Na^{2+}$: 1146.2, found: 1146.5 $[M + 2Na]^{2+}$. Retention time, 13 853 min; HPLC purity, 93.7%.

Fc-SMDC (2). DBCO-amanitin precursor **12** (20 equiv, 12.18 mg) was dissolved in ACN/H_2O (3:1, 1.28 mL) and added to DUPA-Fc **15** (24 mg, 48.6 μM) in PBS buffer (pH 7.4, 8.46 mL). DMSO (2.24 mL) was added and the mixture was incubated at 37 °C for 24 h. Purification was performed by SEC-FPLC. The conjugate was

https://doi.org/10.1021/acs.jmedchem.1c00003
J. Med. Chem. 2021, 64, 4117−4129

concentrated to a final volume of 7.5 mL and filtered through a 0.22 μm sterile filter prior to its use in biological assays. The concentration of conjugate **2** was determined as 3.16 mg/mL (23.7 mg) by $Abs_{280\,nm}$ (MW = 61425.21 Da, ε_{280} = 85 500 cm^{-1} M^{-11}). Retention time, 9.7 min; SEC-HPLC purity, >99%.

*5-Benzyl 1-(tert-butyl) (((S)-1,5-di-tert-butoxy-1,5-dioxopentan-2-yl)carbamoyl)-L-glutamate (**5**).* α,γ-Di-*tert*-butyl L-glutamate (2 g, 6.76 mmol) was added in portions at 0 °C to a solution of disuccinimidyl carbonate (DSC) (1.73 g, 6.76 mmol) in *N*,*N*-dimethylformamide (DMF) (31.6 mL) to form the NHS-activated ester **4**. After 50 min, triethylamine (TEA) (937 μL, 6.76 mmol) was added. After complete conversion, α-*tert*-butyl-γ-benzyl L-glutamate (2.23 g, 6.76 mmol) and TEA (1.87 mL, 13.52 mmol) were added at 0 °C. The reaction mixture was stirred overnight at room temperature. DMF was removed in vacuo and the residue was dissolved in methyl *t*-butyl ether (MTBE) (100 mL). The organic layer was washed with a 15% citric acid solution (2 × 100 mL), water (2 × 100 mL), saturated $NaHCO_3$ solution (2 × 100 mL), and water (80 mL) in sequence. The organic layer was dried over $MgSO_4$, filtered, and concentrated. The resulting yellowish oil was purified by chromatography on a silica gel column with a gradient of 0−33% EtOAc in hexane to provide urea **5** as a colorless syrup (3.02 g, 77%). MS (ESI): *m*/*z* calcd for $C_{30}H_{46}N_2O_9 + H^+$: 579.72 $[M + H]^+$; found: 579.17; calcd for $C_{30}H_{46}N_2O_9 + Na^+$: 601.70 $[M + Na]^+$; found: 601.35; calcd for $C_{60}H_{92}N_4O_{18} + Na^+$: 1180.41 $[2M + Na]^+$; found: 1180.35.

*(S)-5-(tert-Butoxy)-4-(3-((S)-1,5-di-tert-butoxy-1,5-dioxopentan-2-yl)ureido)-5-oxopentanoic Acid (**6**).* Compound **5** (3.02 g, 5.21 mmol) was hydrogenated at room temperature in ethyl acetate (EtOAc) (27.3 mL) and in the presence of Pd-C overnight. Palladium was filtered off, and the filtrate was washed thoroughly with EtOAc. The filtrate was concentrated under reduced pressure to provide DUPA precursor **6** as a clear colorless syrup (2.45 g, 96%). MS (ESI): *m*/*z* calcd for $C_{23}H_{40}N_2O_9 + H^+$: 489.59 $[M + H]^+$; found: 489.20; calcd for $C_{46}H_{82}N_4O_{18} + Na^+$: 978.16 $[2M + Na]^+$; found: 978.22.

*DUPA-8-Aoc-Phe-Phe-Cys-OH (**8**).* Cys-preloaded 2-chlorotrityl (H-Cys(Trt)-2ClTrt) resin (391 mg, 0.25 mmol) was swollen in dimethylformamide (DMF)/dichloromethane (DCM) (1:1) for 30 min prior to use. For each coupling, 2.5 equiv of Fmoc-protected amino acid or **6**, 4.25 equiv of 3-[bis(dimethylamino)methyliumyl]-3*H*-benzotriazol-1-oxide hexafluorophosphate (HBTU), 4.25 equiv of *N*-hydroxybenzotriazole (HOBt), and 8.5 equiv of *N*-ethyl-*N*-(propan-2-yl)propan-2-amine (DIPEA) were used. Each coupling reaction was carried out at 60 °C and 40 W for 10 min. After each coupling reaction, the resin was washed with DCM (×3) and DMF (×3) in sequence. Then, 20% piperidine in DMF was added to the reaction vessel and two deprotection cycles (60 °C, 40 W, 30 s; 60 °C, 40 W, 2.5 min) were performed. After draining, the resin was washed with neat DMF (×3) and DCM (×2). Resin-bound peptide was cleaved with a trifluoroethanol (TFE)/acetic acid (AcOH)/DCM (1:1:8, 10 mL) mixture at 23 °C for 1.5 h. The resin was then washed with fresh TFE/AcOH/DCM (1:1:8) mixture (10 mL, 2 min), DCM (10 mL, 2 min), and methanol (MeOH) (10 mL, 2 min) in sequence. The filtrates were collected and concentrated in vacuo. The peptide was subsequently treated with a trifluoroacetic acid (TFA)/triisopropylsilane(TIS)/H_2O (95:2.5:2.5, 8 mL) and 1,4-dithiothreitol (DTT) (362 mg) mixture and stirred at room temperature under argon for 1.5 h. The mixture was co-evaporated with toluene (2 × 8 mL). Addition of precooled MTBE (40 mL) caused peptide precipitation. The precipitate was isolated by centrifugation at 0 °C, collected, and washed with additional precooled MTBE (40 mL); centrifuged at 0 °C; and collected. The pellet was dissolved in acetonitrile (ACN)/H_2O (1:1, v:v, 2 mL) and purified in portions by preparative RP-HPLC [λ = 210 nm; gradient: 0 min 5% B; 15−18 min 100% B; 18.50−22 min 5% B; A = water with 0.05% TFA, B = acetonitrile; flow rate: 30 mL/min]. Fractions corresponding to the target compound were combined, evaporated, and lyophilized overnight from *tert*-butanol (^{t}BuOH)/H_2O (4:1, v:v, 5 mL) to afford reagent **8** as a white powder (122.9 mg, 85%). MS (ESI): *m*/*z* calcd for $C_{40}H_{54}N_6O_{13}S + H^+$: 859.98 $[M + H]^+$; found: 859.33; calcd for $C_{40}H_{54}N_6O_{13}S + Na^+$: 881.96 $[M + Na]^+$; found: 881.33.

*Boc-Val-Ala-PAB-α-amanitin (**11**).* Vacuum-dried α-amanitin (57 mg, 0.062 mmol) was dissolved in dry dimethyl acetamide (DMA; 3 mL) under argon at room temperature. Boc-Val-Ala(SEM)-PAB-Br linker **10** (145.5 mg, 0.248 mmol) and 0.2 M solution of cesium carbonate (Cs_2CO_3) (372.2 μL, 0.074 mmol) were added. After 4 h at room temperature, the reaction mixture was acidified to pH 5 with AcOH. The solvent was removed in vacuo, and the residue was purified by RP-HPLC (λ = 305 nm; gradient: 0−5 min 5% B; 20−25 min 100% B; 27−35 min 5% B; A = water; B = MeOH). The solvents were then evaporated to dryness, affording **11** as a colorless solid (54.46 mg, 62%). MS (ESI): *m*/*z* calcd for $C_{65}H_{97}N_{13}O_{19}SSi + H^+$: 1425.70 $[M + H]^+$; found: 1425.23.

DBCO-Val-Ala-PAB-O-α-amanitin (12). α-Amanitin precursor **S-17** (80.32 mg, 0.067 mmol) was dissolved in absolute DMF (1.6 mL). Dibenzocyclooctine-*N*-succinimidyl ester (DBCO-SE) (29.8 mg, 0.074 mmol) dissolved in DMF (1.6 mL) and DIPEA (22.9 μL, 0.13 mmol) was added to the solution. The reaction mixture was stirred at rt for 2.5 h.

The reaction was quenched by adding H_2O (100 μL), and DMF was evaporated in vacuo. The residue was dissolved in methanol (MeOH) (2 mL) and dripped into precooled MTBE (40 mL) and centrifuged at 0 °C. The pellet was washed with MTBE (40 mL), collected, and dried in vacuo. The compound was purified by RP-HPLC [λ = 305 nm; gradient: 0−15 min 5% B; 18 min 100% B; 1.5−22 min 5% B; A = water with 0.05% TFA, B = ACN; flow rate: 30 mL/min]. Fractions corresponding to the product were directly lyophilized affording **12** (77.88 mg, 78%) as a white powder. MS (ESI): *m*/*z* calcd for $C_{73}H_{88}N_{14}O_{18}S + H^+$: 1482.67 $[M + H]^+$; found: 1481.42; calcd for $C_{73}H_{88}N_{14}O_{18}S + 2H^{2+}$: 741.84 $[M + 2H]^{2+}$; found: 741.42.

*Maleimidocaproyl-Val-Ala-PAB-α-amanitin (**13**).* NH_2-Val-Ala-PAB-α-amanitin **17** (10.0 mg, 0.0076 mmol) was dissolved in dry DMF (200 μL). ECMS (4.69 mg, 0.015 mmol), dissolved in DMF (104 μL), and DIPEA (5.18 μL, 0.0304 mmol) were added. After 1 h at room temperature under argon, the mixture was dripped into precooled MTBE (40 mL) and centrifuged at 0 °C. The precipitate was collected, washed with MTBE (40 mL), centrifuged, and collected. The crude product was dried in vacuo and purified by RP-HPLC [λ = 305 nm; gradient: 0−5 min 5% B; 20−25 min 100% B; 27−35 min 5% B; A = water with 0.05% TFA; B = MeOH with 0.05% TFA]. Upon freeze-drying, the title compound was obtained as a colorless powder (4.22 mg, 40%). MS (ESI): *m*/*z* calcd for $C_{64}H_{86}N_{14}O_{19}S^+$: 1387.52 $[M]^+$; found: 1387.42; $C_{64}H_{86}N_{14}O_{19}S + 2H^{2+}$: 694.79 $[M + 2H]^{2+}$; found: 694.33; $C_{64}H_{86}N_{14}O_{19}S + H^+ + K^+$: 713.83 $[M + H + K]^{2+}$; found: 713.33.

*DUPA-8-Aoc-Phe-Phe-$(EG_3)_2$-Orn(N_3)-Lys(Gly_3)-NH_2 (**15**).* AmphiSpheres 40 RAM resin (703 mg, 0.267 mmol) was swollen 1 h in DCM, washed with, and resuspended in DMF for 30 min. The resin was deprotected with 20% piperidine in DMF (30 s, rt à 2 min, 30 W, 50 °C) and then shaken with Fmoc-Lys(Mtt)-OH (4.0 equiv), TBTU (3.99 equiv), and DIPEA (8.0 equiv) in DMF (8 mL) for 1 h at rt and then under MW irradiation (30 W, 50 °C, 3 min). Coupling was repeated twice with several DMF washings in between. Fmoc was removed by suspending the resin in 20% piperidine in DMF (3 mL) under the conditions described above. Each coupling was then performed by shaking the resin with the Fmoc-protected amino acid (4.0 equiv), TBTU (3.99 equiv), and DIPEA (8.0 equiv) in DMF (8 mL) under MW irradiation (30 W, 50 °C, 3 min, ×3), followed by Fmoc-removal with the conditions mentioned herein. The protected DUPA reagent **6** (3.0 equiv) was coupled using TBTU (2.99 equiv) and DIPEA (6.0 equiv) under MW irradiation (30 W, 50 °C, 3 min, ×3). Prior to cleavage, Mtt was removed by suspending the resin-bound peptide in DCM/TIS/TFA (97:2:1, 4 mL) and shaking at rt for 10 min. The procedure was repeated till no Mtt-OH could be detected in the filtrate by HPLC (approx. 20 cycles). Afterward, coupling with Fmoc-Gly_3-OH (4.0 equiv), TBTU (3.99 equiv), and DIPEA (8.0 equiv) in DMF (8 mL) was carried out under MW irradiation (30 W, 50 °C, 3 min, ×3), followed by Fmoc-removal with

https://doi.org/10.1021/acs.jmedchem.1c00003
J. Med. Chem. 2021, 64, 4117−4129

the conditions mentioned herein. The resin was then extensively washed with DCM and dried in vacuo. The peptide was cleaved from the resin and totally deprotected with a TFA/anisole/TIS/H_2O (94:2:2:2, 20 mL) cocktail for 2 h at rt. The mixture was precipitated in four portions in precooled MTBE (40 mL/each), and the pellets were collected by centrifugation at 0 °C for 10 min. The pellets were collected, dried in vacuo, and dissolved in ACN/H_2O (1:1, v−v) for purification by RP-HPLC [λ = 210 nm; gradient: 0 min 5% B; 14 min 40% B; 19 min 45% B; 20−21 min 100% B; 22 min 5% B; A = water with 0.05% TFA, B = ACN; flow rate: 30 mL/min]. The desired compound was directly lyophilized affording **15** as a white powder (119.46 mg, 28%). MS (ESI): *m/z* calcd for $C_{72}H_{113}N_{17}O_{24}$ − H^-: 1599.79 $[M - H]^-$; found: 1598.83; calcd for $C_{72}H_{113}N_{17}O_{24}$ − $2H^{2-}$: 799.39 $[M - 2H]^{2-}$; found: 799.00.

*DUPA-Pep-Fc (**16**).* Fc-LPETGG **14** (40 mg, 20.65 μM) was mixed with the peptide sequence **15** (50 equiv, 1 mM) in SrtA reaction-buffer (Tris-HCl 50 mM pH 7.5, NaCl 150 mM, $CaCl_2$ 5 mM) in the presence of a SrtA pentamutant (eSrtA) enzyme (0.125 equiv, 2.6 μM). The reaction was allowed to proceed for 18 h at 25 °C and then purified using SEC-FPLC to remove eSrtA and excess of the peptide. The column was first equilibrated with PBS buffer (pH 7.4), and then DUPA-Fc **16** was eluted using the same buffer as used for column equilibration. The flow-through from the column was concentrated and filtered through a sterile filter. The concentration of DUPA-Fc conjugate **16** was determined as 3.6 mg/mL (27.87 mg) by $Abs_{280\,nm}$ (MW = 58461.89 Da, ε_{280} = 74675.1 cm^{-1} M^{-11}). Retention time, 9.4 min; SEC-HPLC purity, 99%.

*NH_2-Val-Ala-PAB-α-amanitin (**17**).* Boc-Val-Ala-PAB-α-amanitin **11** (134.29 mg, 0.0943 mmol) was dissolved in TFA (4.98 mL) and stirred at room temperature for 2 min and then concentrated to dryness. The residue was dissolved in water (4.98 mL), and the pH was adjusted to 10 with a 3.2% NH_3 aqueous solution added dropwise. The resulting suspension was freeze-dried and the resulting powder was purified by preparative RP-HPLC (λ = 305 nm; gradient: 0−2 min 5% B; 2−10 min 20% B; 10−10.5 min 25% B; 10.5−13 min 100% B; 13−14 min 5% B; A = water with 0.05% TFA; B = ACN). Upon elution, the title compound was directly freeze-dried overnight and obtained as a colorless powder (68.59 mg, 55%). MS (ESI): *m/z* calcd for $C_{54}H_{75}N_{13}O_{16}S$ + H^+: 1194.53 $[M + H]^+$; found: 1194.8; calcd for $C_{54}H_{75}N_{13}NaO_{16}S$ + Na^+: 1216.51 $[M + Na]^+$; found: 1217.8.

***In Vitro* Cytotoxicity Assay.** LNCaP cells were cultivated in RPMI medium and PC3 cells in DMEM (PAN-Biotech GmbH) supplemented with 10% fetal bovine serum L-glutamine, 100 units of penicillin/mL, and 100 μg/mL streptomycin. Cells were incubated at 37 °C in 100% humidity and 5% CO_2 saturation. For the cytotoxicity assay, 2 × 10^3 cells/well were plated in 96-well black clear bottom plates (PerkinElmer) in 90 μL of the medium and allowed to attach for 16 h. A panel of eight serial dilutions of the test compounds was prepared in cell culture media, and 10 μL was added to each well and incubated for an additional 96 h. Next, 100 μL of CellTiterGlo 2.0 reagent (Promega) was added directly to the cell culture media and incubated for 10 min to allow for cell lysis. Luminescence signal intensities were measured using a microplate reader (Fluostar Optima BMG Labtec). The background was determined from wells containing the medium only with CellTiterGlo 2.0 reagent and subtracted from each value. *In vitro* competitive cytotoxic assay was performed in the presence of 100 × molar excess of 2-PMPA over HDP 30.2284 (SMDC) and 200 × molar excess of 2-PMPA over HDP 30.2972 (Fc-SMDC).

Determination of the Maximum Tolerated Dose. All experiments were carried out following the guidelines of the German Animal Welfare Act and all relevant laws and regulations. Protocols were approved by the local regulatory authority (Regierungspräsidium Karlsruhe, Germany, file numbers: 35-9185.82/A-22/15, 35-9185.81/G-197/15, 35-9185.81/G-13/16, and 35-9185.81/G-157/17). The tolerability of compounds was tested in 6−8 week old CB17-Scid male mice. The conjugates were diluted in PBS (pH 7.4) containing a maximal concentration of 5% DMSO. Survival and clinical signs were determined daily. The body weight was determined twice a week. Three animals per group were injected with a doubling increasing dose from a dose with no effect until clinical signs such as net body weight loss of more than 20%; lack of recovery; and/or one of the following symptoms of lack of motility, hind leg paralysis, cachexia, poor general health condition, or general signs of pain occurred.

***In Vivo* Efficacy Studies.** 6−8 week old CB17-Scid male mice animals were subcutaneously inoculated with 2.5 × 10^6 LNCaP tumor cells in 200 μL of a 1:1 mixture of red phenol-free RPMI (Gibco) and Matrigel (Corning) into the right flank. The therapy was started once a mean tumor volume reached approx. 100 mm^3. The compounds were administered at doses and frequencies based on the findings of toxicity and pharmacokinetic studies. Tumors were measured using external calipers at least twice per week.

***In Vivo* Pharmacokinetic and Biodistribution Study.** LNCaP tumor-bearing CB17-Scid male mice were injected with 4× MTDs of HDP 30.2284 (0.184 mg/kg) and 1× MTD HDP 30.2972 (1.0 mg/kg). The animals were sacrificed at predefined time-points. The serum, tumor, kidney, and liver were isolated, snap-frozen in liquid nitrogen, and stored at −70 °C.

Competitive Anti-α-amanitin ELISA. Approximately 100 mg of tissue was transferred to a FastPrep tube (MP Biomedicals). A triple volume of mixed gender mouse serum (Seralab) with respect to the mass of the organ was added to the tube. One steel grinding ball (MP Biomedicals) was added to each tube, and the samples were homogenized using a planetary ball mill (Precellys 24 Tissue Homogenizer, Bertin Instruments). The homogenate was centrifuged for 5 min at 14 000 rpm and 4 °C (Thermo Fischer Scientific, Tabletop centrifuge FRESCO 17), and the supernatants were collected. For competitive α-amanitin ELISA, 60 μL of the tissue supernatant or 60 μL of the mouse serum collected in the pharmacokinetic study was precipitated with 240 μL of 100% ethanol and incubated for 20 min at −20 °C to ensure complete protein precipitation. After centrifugation, the supernatants were collected and evaporated using a rotational vacuum concentrator (Martin Christ GmbH) for 3 h at 1300 rpm and 53 °C. For determination of standard curves, reference solutions of α-amanitin and HDP 30.2284 ranging from 0.4 to 8100 nM were prepared in the mouse serum. The mouse serum containing the highest DMSO concentration was used as the blank. Then, 60 μL of the standard solutions and the blank were precipitated and processed as described above.

ELISA plates were coated overnight with 50 μL of the anti-α-amanitin capture serum (Polyclonal rabbit, Heidelberg Pharma Research GmbH), *c* = 6.67 μg/mL diluted in PBS. The plates were blocked with 200 μL/well ELISA blocking buffer (3% BSA/PBS-solution) for 1 h at 100 rpm and 37 °C and washed with 300 μL/well wash buffer (0.05% Tween/PBS) using an automated Hydrospeed ELISA Washer (Tecan). Evaporated samples prepared as described above were reconstituted in the ELISA sample buffer (1% BSA/PBS with 20% EtOH) and mixed with 50 μL of 1 nM biotin-α-amanitin conjugate (Heidelberg Pharma Research GmbH) also reconstituted in the ELISA sample buffer. Then, 50 μL of the 1:1 mixture of sample and biotinylated α-amanitin was applied onto the ELISA plate in duplicate and incubated for 1 h at 37 °C. The plate was washed three times with 300 μL of the ELISA wash buffer using an automated Hydrospeed ELISA Washer (Tecan). Subsequently 50 μL of streptavidin-HRP (1 μg/mL) was added in each well and incubated for 1 h at 100 rpm and 37 °C. After washing, 100 μL of 0.1 mg/mL TMB reagent reconstituted in 0.1 M sodium acetate buffer containing 0.001% H_2O_2 was added. After 15 min, the reaction was stopped with 50 μL of 1 M H_2SO_4. Absorbance was measured at 450 nm and corrected with the background absorbance at 570 nm (Fluostar Optima BMG Labtec). The concentration of α-amanitin-containing compounds was calculated based on the interpolation of the sigmoidal standard curve using GraphPad Prism 7.0 software, and for organs and tumor, the calculation was based on the mass of the analyzed tissue.

Sandwich ELISA for Determination of HDP 30.2972 Concentration. ELISA was performed as described above with the following changes. HDP 30.2972 standards were prepared in the sample buffer (Candor Biosciences GmbH) as 1:2 serial dilutions

https://doi.org/10.1021/acs.jmedchem.1c00003
J. Med. Chem. 2021, 64, 4117−4129

ranging from 1.6 to 400 pM. Standards were analyzed in parallel with the serum and organ extracts. Sera and organ extracts were diluted in the sample buffer (Candor Biosciences GmbH) in two steps, (1) 1:100 and (2) 1:10, to reach a final dilution of 1:1000. Next, 50 μL of each sample was applied in duplicate on the ELISA plate coated with α-amanitin capture serum and incubated at 37 °C for 1 h on an orbital microplate shaker at 100 rpm. After washing 50 μL of a 1:10 000 dilution of secondary antibody rabbit anti-Human-IgG-HRP (Abcam ab98576) reconstituted in sample buffer was added per well and incubated for 1 h, 100 rpm, at 37 °C.

Statistical Analysis. The sample size was empirically set at $n = 3$ for *in vitro* cell experiments, $n = 3$ for *in vivo* biodistribution and pharmacokinetic studies, and $n = 8-10$ for *in vivo* efficacy studies. Determination of IC_{50} values was done using GraphPad Prism 7.0 software. The Mann−Whitney test was used to compare the different experimental arms *in vivo*. The level of significance was set at values $^{*}P < 0.05$, $^{**}P < 0.01$, and $^{***}P < 0.001$. The concentration of compounds was calculated based on the interpolated standard curves. The half-lifetime of small molecular conjugate HDP 30.2284 was calculated using a one-phase decay exponential nonlinear regression curve fit. The half-lifetime of HDP 30.2972 (Fc-SMDC) was calculated based on a two-phase decay nonlinear regression curve fit.

■ ASSOCIATED CONTENT

Supporting Information

The Supporting Information is available free of charge at https://pubs.acs.org/doi/10.1021/acs.jmedchem.1c00003.

Supplementary materials and methods; general synthesis of α-amantin derivatives 12 and 13; synthesis of Boc-Val-Ala(SEM)-PAB-Br linker 10; cloning of plasmid for protein expression; expression and purification of protein Fc-LPETGG (14); and production of eSrtA enzyme; Supplementary figures: Figure S1: RP-HPLC trace of pure SMDC (1); Figure S2: SEC-HPLC trace of purified DUPA-Fc (16); Figure S3: SEC-HPLC trace of purified DUPA-Fc-amanitin HDP 30.2972 (2); Figure S4: Cytotoxicity of DUPA-alpha-amanitin SMDC HDP 30.2284; Fc analogue HDP 30.2972 and unconjugated alpha-amanitin in PSMA negative (PSMA -) PC3 cell line (PDF)

■ AUTHOR INFORMATION

Corresponding Author

Andreas Pahl − *Heidelberg Pharma Research GmbH, Heidelberg Pharma AG, 68526 Ladenburg, Germany;* orcid.org/0000-0002-6294-0335; Email: andreas.pahl@hdpharma.com

Authors

Francesca Gallo − *Heidelberg Pharma Research GmbH, Heidelberg Pharma AG, 68526 Ladenburg, Germany*

Barbara Korsak − *Heidelberg Pharma Research GmbH, Heidelberg Pharma AG, 68526 Ladenburg, Germany*

Christoph Müller − *Heidelberg Pharma Research GmbH, Heidelberg Pharma AG, 68526 Ladenburg, Germany*

Torsten Hechler − *Heidelberg Pharma Research GmbH, Heidelberg Pharma AG, 68526 Ladenburg, Germany*

Desislava Yanakieva − *Department of Biochemistry, Technical University of Darmstadt, 64287 Darmstadt, Germany*

Olga Avrutina − *Department of Biochemistry, Technical University of Darmstadt, 64287 Darmstadt, Germany*

Harald Kolmar − *Department of Biochemistry, Technical University of Darmstadt, 64287 Darmstadt, Germany*

Complete contact information is available at: https://pubs.acs.org/10.1021/acs.jmedchem.1c00003

Author Contributions

[§]F.G. and B.K. contributed equally to this work. All authors have given approval to the final version of the manuscript.

Notes

The authors declare the following competing financial interest(s): A.P. is a full-time employee of Heidelberg Pharma AG, F.G., B.K., T.H., and C.M. are full-time employees of Heidelberg Pharma Research GmbH. Heidelberg Pharma Research GmbH is a German biotech company operating in the field of antibody-drug conjugates and is a daughter company of Heidelberg Pharma AG. A.P. and T.H. are shareholders of Heidelberg Pharma AG.

■ ACKNOWLEDGMENTS

F.G. and B.K. acknowledge the European Union within the H2020 Marie Skłodowska-Curie European Training Network MAGICBULLET (MSCA-ITN-2014-ETN, grant agreement number 642004).

■ ABBREVIATIONS

SMDC, small-molecule drug conjugate; ADC, antibody drug conjugate; MTD, maximum tolerated dose

■ REFERENCES

(1) Abdollahpour-Alitappeh, M.; Lotfinia, M.; Larki, P.; Faghfourian, B.; Sepehr, K. S.; Abbaszadeh-Goudarzi, K.; Abbaszadeh-Goudarzi, G.; Johari, B.; Zali, M. R.; Bagheri, N.; et al. Antibody-drug conjugates (ADCs) for cancer therapy: Strategies, challenges, and successes. *J. Cell. Physiol.* **2019**, *234*, 5628−5642.

(2) Amiri-Kordestani, L.; Blumenthal, G. M.; Xu, Q. C.; Zhang, L.; Tang, S. W.; Ha, L.; Weinberg, W. C.; Chi, B.; Candau-Chacon, R.; Hughes, P.; Russell, A. M.; Miksinski, S. P.; Chen, X. H.; McGuinn, W. D.; Palmby, T.; Schrieber, S. J.; Liu, Q.; Wang, J.; Song, P.; Mehrotra, N.; Skarupa, L.; Clouse, K.; Al-Hakim, A.; Sridhara, R.; Ibrahim, A.; Justice, R.; Pazdur, R.; Cortazar, P. FDA approval: ado-trastuzumab emtansine for the treatment of patients with HER2-positive metastatic breast cancer. *Clin. Cancer Res.* **2014**, *20*, 4436−4441.

(3) Tsumura, R.; Manabe, S.; Takashima, H.; Koga, Y.; Yasunaga, M.; Matsumura, Y. Influence of the dissociation rate constant on the intra-tumor distribution of antibody-drug conjugate against tissue factor. *J. Controlled Release* **2018**, *284*, 49−56.

(4) Leamon, C. P.; Reddy, J. A.; Vetzel, M.; Dorton, R.; Westrick, E.; Parker, N.; Wang, Y.; Vlahov, I. Folate targeting enables durable and specific antitumor responses from a therapeutically null tubulysin B analogue. *Cancer Res.* **2008**, *68*, 9839−9844.

(5) Kularatne, S. A.; Wang, K.; Santhapuram, H. K.; Low, P. S. Prostate-specific membrane antigen targeted imaging and therapy of prostate cancer using a PSMA inhibitor as a homing ligand. *Mol. Pharm.* **2009**, *6*, 780−789.

(6) Leamon, C. P.; Reddy, J. A.; Bloomfield, A.; Dorton, R.; Nelson, M.; Vetzel, M.; Kleindl, P.; Hahn, S.; Wang, K.; Vlahov, I. R. Prostate-Specific Membrane Antigen-Specific Antitumor Activity of a Self-Immolative Tubulysin Conjugate. *Bioconjugate Chem.* **2019**, *30*, 1805−1813.

(7) Ginj, M.; Zhang, H.; Waser, B.; Cescato, R.; Wild, D.; Wang, X.; Erchegyi, J.; Rivier, J.; Macke, H. R.; Reubi, J. C. Radiolabeled somatostatin receptor antagonists are preferable to agonists for in vivo peptide receptor targeting of tumors. *Proc. Natl. Acad. Sci. U.S.A.* **2006**, *103*, 16436−16441.

(8) Cazzamalli, S.; Corso, D.; Widmayer, A.; Neri, F. D. Chemically Defined Antibody- and Small Molecule-Drug Conjugates for in Vivo Tumor Targeting Applications: A Comparative Analysis. *J. Am. Chem. Soc.* **2018**, *140*, 1617−1621.

(9) Roopenian, D. C.; Akilesh, S. FcRn: the neonatal Fc receptor comes of age. *Nat. Rev. Immunol.* **2007**, *7*, 715−725.
(10) Molineux, G.; Newland, A. Development of romiplostim for the treatment of patients with chronic immune thrombocytopenia: from bench to bedside. *Br. J. Haematol.* **2010**, *150*, 9−20.
(11) Schifferli, A.; Nimmerjahn, F.; Kuhne, T. Immunomodulation in Primary Immune Thrombocytopenia: A Possible Role of the Fc Fragment of Romiplostim? *Front. Immunol.* **2019**, *10*, No. 1196.
(12) Sokoloff, R. L.; Norton, K. C.; Gasior, C. L.; Marker, K. M.; Grauer, L. S. A dual-monoclonal sandwich assay for prostate-specific membrane antigen: levels in tissues, seminal fluid and urine. *Prostate* **2000**, *43*, 150−157.
(13) Silver, D. A.; Pellicer, I.; Fair, W. R.; Heston, W. D.; Cordon-Cardo, C. Prostate-specific membrane antigen expression in normal and malignant human tissues. *Clin. Cancer Res.* **1997**, *3*, 81−85.
(14) Phase 1 of EC1169 In Patients With Recurrent MCRPC. https://clinicaltrials.gov/ct2/show/NCT02202447.
(15) Petrylak, D. P.; Kantoff, P.; Vogelzang, N. J.; Mega, A.; Fleming, M. T.; Stephenson, J. J., Jr; Frank, R.; Shore, N. D.; Dreicer, R.; McClay, E. F.; Berry, W. R.; Agarwal, M.; DiPippo, V. A.; Rotshteyn, Y.; Stambler, N.; Olson, W. C.; Morris, S. A.; Israel, R. J. Phase 1 study of PSMA ADC, an antibody-drug conjugate targeting prostate-specific membrane antigen, in chemotherapy-refractory prostate cancer. *Prostate* **2019**, *79*, 604−613.
(16) Milowsky, M. I.; Galsky, M. D.; Morris, M. J.; Crona, D. J.; George, D. J.; Dreicer, R.; Tse, K.; Petruck, J.; Webb, I. J.; Bander, N. H.; Nanus, D. M.; Scher, H. I. Phase 1/2 multiple ascending dose trial of the prostate-specific membrane antigen-targeted antibody drug conjugate MLN2704 in metastatic castration-resistant prostate cancer. *Urol. Oncol.* **2016**, *34*, 530.e15−530.e21.
(17) Yaghoubi, S.; Karimi, M. H.; Lotfinia, M.; Gharibi, T.; Mahi-Birjand, M.; Kavi, E.; Hosseini, F.; Sineh Sepehr, K.; Khatami, M.; Bagheri, N.; Abdollahpour-Alitappeh, M. Potential drugs used in the antibody-drug conjugate (ADC) architecture for cancer therapy. *J. Cell. Physiol.* **2020**, *235*, 31−64.
(18) Pahl, A.; Lutz, C.; Hechler, T. Amanitins and their development as a payload for antibody-drug conjugates. *Drug Discovery Today: Technol.* **2018**, *30*, 85−89.
(19) Kularatne, S. A.; Zhou, Z.; Yang, J.; Post, C. B.; Low, P. S. Design, synthesis, and preclinical evaluation of prostate-specific membrane antigen targeted (99m)Tc-radioimaging agents. *Mol. Pharm.* **2009**, *6*, 790−800.
(20) Kuester, D.; Lippert, H.; Roessner, A.; Krueger, S. The cathepsin family and their role in colorectal cancer. *Pathol., Res. Pract.* **2008**, *204*, 491−500.
(21) Ruan, H.; Hao, S.; Young, P.; Zhang, H. Targeting Cathepsin B for Cancer Therapies. *Horiz. Cancer Res.* **2015**, *56*, 23−40.
(22) Alley, S. C.; Benjamin, D. R.; Jeffrey, S. C.; Okeley, N. M.; Meyer, D. L.; Sanderson, R. J.; Senter, P. D. Contribution of linker stability to the activities of anticancer immunoconjugates. *Bioconjugate Chem.* **2008**, *19*, 759−765.
(23) Thomas, J. D.; Cui, H.; North, P. J.; Hofer, T.; Rader, C.; Burke, T. R., Jr. Application of strain-promoted azide-alkyne cycloaddition and tetrazine ligation to targeted Fc-drug conjugates. *Bioconjugate Chem.* **2012**, *23*, 2007−2013.
(24) Swee, L. K.; Guimaraes, C. P.; Sehrawat, S.; Spooner, E.; Barrasa, M. I.; Ploegh, H. L. Sortase-mediated modification of αDEC205 affords optimization of antigen presentation and immunization against a set of viral epitopes. *Proc. Natl. Acad. Sci. U.S.A.* **2013**, *110*, 1428−1433.
(25) Wagner, K.; Kwakkenbos, M. J.; Claassen, Y. B.; Maijoor, K.; Bohne, M.; van der Sluijs, K. F.; Witte, M. D.; van Zoelen, D. J.; Cornelissen, L. A.; Beaumont, T.; Bakker, A. Q.; Ploegh, H. L.; Spits, H. Bispecific antibody generated with sortase and click chemistry has broad antiinfluenza virus activity. *Proc. Natl. Acad. Sci. U.S.A.* **2014**, *111*, 16820−16825.
(26) Kornberger, P.; Skerra, A. Sortase-catalyzed in vitro functionalization of a HER2-specific recombinant Fab for tumor targeting of the plant cytotoxin gelonin. *mAbs* **2014**, *6*, 354−366.
(27) Dickgiesser, S.; Rasche, N.; Nasu, D.; Middel, S.; Horner, S.; Avrutina, O.; Diederichsen, U.; Kolmar, H. Self-Assembled Hybrid Aptamer-Fc Conjugates for Targeted Delivery: A Modular Chemoenzymatic Approach. *ACS Chem. Biol.* **2015**, *10*, 2158−2165.
(28) Lee, S.; Lee, Y.; Kim, H.; Lee, D. Y.; Jon, S. Bilirubin Nanoparticle-Assisted Delivery of a Small Molecule-Drug Conjugate for Targeted Cancer Therapy. *Biomacromolecules* **2018**, *19*, 2270−2277.
(29) Perrino, E.; Steiner, M.; Krall, N.; Bernardes, G. J.; Pretto, F.; Casi, G.; Neri, D. Curative properties of noninternalizing antibody-drug conjugates based on maytansinoids. *Cancer Res.* **2014**, *74*, 2569−2578.
(30) Dal Corso, A.; Gebleux, R.; Murer, P.; Soltermann, A.; Neri, D. A non-internalizing antibody-drug conjugate based on an anthracycline payload displays potent therapeutic activity in vivo. *J. Controlled Release* **2017**, *264*, 211−218.
(31) Lv, Q.; Yang, J.; Zhang, R.; Yang, Z.; Yang, Z.; Wang, Y.; Xu, Y.; He, Z. Prostate-Specific Membrane Antigen Targeted Therapy of Prostate Cancer Using a DUPA-Paclitaxel Conjugate. *Mol. Pharm.* **2018**, *15*, 1842−1852.
(32) Cazzamalli, S.; Corso, A. D.; Neri, D. Linker stability influences the anti-tumor activity of acetazolamide-drug conjugates for the therapy of renal cell carcinoma. *J. Controlled Release* **2017**, *246*, 39−45.
(33) Moshnikova, A.; Moshnikova, V.; Andreev, O. A.; Reshetnyak, Y. K. Antiproliferative effect of pHLIP-amanitin. *Biochemistry* **2013**, *52*, 1171−1178.
(34) Bodero, L.; Lopez Rivas, P.; Korsak, B.; Hechler, T.; Pahl, A.; Muller, C.; Arosio, D.; Pignataro, L.; Gennari, C.; Piarulli, U. Synthesis and biological evaluation of RGD and isoDGR peptidomimetic-alpha-amanitin conjugates for tumor-targeting. *Beilstein J. Org. Chem.* **2018**, *14*, 407−415.
(35) Wang, Y. M. C.; Sloey, B.; Wong, T.; Khandelwal, P.; Melara, R.; Sun, Y. N. Investigation of the pharmacokinetics of romiplostim in rodents with a focus on the clearance mechanism. *Pharm. Res.* **2011**, *28*, 1931−1938.
(36) Wu, B.; Johnson, J.; Soto, M.; Ponce, M.; Calamba, D.; Sun, Y. N. Investigation of the mechanism of clearance of AMG 386, a selective angiopoietin-1/2 neutralizing peptibody, in splenectomized, nephrectomized, and FcRn knockout rodent models. *Pharm. Res.* **2012**, *29*, 1057−1065.
(37) Letschert, K.; Faulstich, H.; Keller, D.; Keppler, D. Molecular characterization and inhibition of amanitin uptake into human hepatocytes. *Toxicol. Sci.* **2006**, *91*, 140−149.
(38) Chatalic, K. L.; Heskamp, S.; Konijnenberg, M.; Molkenboer-Kuenen, J. D.; Franssen, G. M.; Clahsen-van Groningen, M. C.; Schottelius, M.; Wester, H. J.; van Weerden, W. M.; Boerman, O. C.; de Jong, M. Towards Personalized Treatment of Prostate Cancer: PSMA I&T, a Promising Prostate-Specific Membrane Antigen-Targeted Theranostic Agent. *Theranostics* **2016**, *6*, 849−861.
(39) Zhang, D.; Dragovich, P. S.; Yu, S. F.; Ma, Y.; Pillow, T. H.; Sadowsky, J. D.; Su, D.; Wang, W.; Polson, A.; Khojasteh, S. C.; Hop, C. Exposure-Efficacy Analysis of Antibody-Drug Conjugates Delivering an Excessive Level of Payload to Tissues. *Drug Metab. Dispos.* **2019**, *47*, 1146−1155.

https://doi.org/10.1021/acs.jmedchem.1c00003
J. Med. Chem. 2021, 64, 4117−4129